NEW MEXICO TECH
SCIENCE • ENGINEERING • RESEARCH • UNIVERSITY

SAND2020-0249PE

Karlsruher Institut für Technologie

Corrosion of C1018 Steel Under WIPP Conditions

Chase Kicker

New Mexico Tech Department of
Materials and Metallurgical Engineering

PRESENTED BY

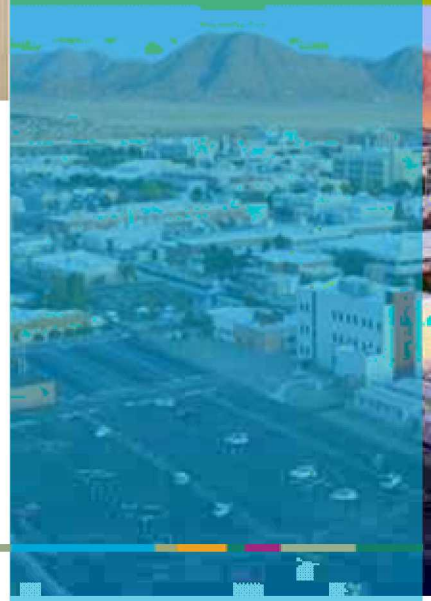

Sandia National Laboratories is a multimission laboratory managed and operated by National Technology & Engineering Solutions of Sandia, LLC, a wholly owned subsidiary of Honeywell International Inc., for the U.S. Department of Energy's National Nuclear Security Administration under contract DE-NA0003525.

This research is funded by WIPP programs administered by the Office of Environmental Management (EM) of the U.S Department of Energy.

Waste Isolation Pilot Plat (WIPP)

- Deep geologic repository for transuranic (TRU) waste
- TRU waste is stored 660m underground in the 380m thick Salado formation
- First barrel of waste was placed underground in 1999.

Remote-Handled Waste

Contact-Handled Waste

http://www.wipp.energy.gov/wipprecovery/about.html

Introduction

- Goal of WIPP - safe storage of nuclear waste for 10,000 years
- ~65,000 metric tons of steel present
- Element interactions must be modeled
- Steel will begin corroding immediately

Introduction

- Steel corrosion could produce significant hydrogen gas generation
- Corrosion rate and mechanisms must be determined
- Various rate determination methods
- Static, Flow-through, and Electrochemical set-ups

Corrosion

- Corrosion accelerated by salt environment
- Once vault is sealed, corrosion process will expend all oxygen
- Corrosion shifts to anaerobic mechanism
- Corrosion process produces hydrogen gas

Corrosion

- Relationship between chloride bearing high ionic strength solutions and corrosion must be better understood
- Effects of sulfide in this environment must also be understood
- Sulfide corrosion products vary and create a number of different passive layers

Corrosion

- Depending on the corrosion mechanism, the stoichiometry of hydrogen production relative to amount of iron will change

Iron (II) Hydroxide Reaction: $Fe°(s) + 2H_2O(l) = Fe(OH)_2(s) + H_2(g)$

Magnetite Reaction: $3Fe°(s) + 4H_2O(l) = Fe_3O_4(s) + 4H_2(g)$

Corrosion

- When sulfide is introduced, there are several potential mechanisms. Mackinawite (FeS_{1-x}) subsequently transforms from its amorphous phase to Troilite, Pyrite, Greigite, and finally Pyrrhotite.

Troilite Reaction: $Fe°(s) + H_2S(aq) = FeS(s) + H_2(g)$

Pyrite Reaction: $Fe°(s) + 2H_2S(aq) = FeS_2(s) + 2H_2(g)$

Greigite Reaction: $3Fe°(s) + 4H_2S(aq) = Fe_3S_4(s) + 4H_2(g)$

Pyrrhotite Reaction: $7Fe°(s) + 8H_2S(aq) = Fe_7S_8(s) + 8H_2(g)$

Previous Research

- Tests in simulated Salado brine used hydrogen gas evolution to calculate a corrosion rate of 0.71 μm/yr at room temperature. (Telander and Westerman 1993)

- Carbon steel corrosion tests in pure water at room temperature yielded about 0.02 μm/yr , but the addition of chlorides caused an increase to 0.1 μm/yr. (Kaneko et. al. 2004)

Previous Research

- Carbon steel electrochemical measurements at room temperature resulted in rates between 10-20 μm/yr (Sherar et. al. 2010)

- The addition of sulfide in saline solutions at room temperature resulted in rates of 700 μm/yr determined by weight loss (Liu et. al. 2014)

Previous Research

- Electrochemical tests of low carbon steel at 90°C reported rates of 95 μm/yr in the first months of testing before tapering off to near zero (Schlegel et. al. 2014)

Materials

- C1018 steel was used to simulate average composition of the waste containers

Table 1. *Chemical Composition of the C1018 steel as provided by Alabama Specialty Products determined by ASTM-A108.*

Element	Fe	C	Mn	P	S	Si	Cu	Ni	Cr	Mo
Concentration (wt.%)	98.72	0.184	0.75	0.011	0.014	0.017	0.10	0.08	0.10	0.023

Solutions

- Solutions for the Static and Flow-Through experiments were prepared inside a glovebox under a nitrogen atmosphere.

- Simplified Generic Weep Brine (SGWB) consists of 3.5 m NaCl and 1 m $MgCl_2 \cdot 6H_2O$

Static Reactors

- Static tests constructed to allow for corrosion product formation and hydrogen gas formation
- Steel coupons were submerged in SGWB and sealed with a pressure gauge
- Tests run for several months at 90˚C

Static Reactors

Figure 1. A. *Static reactor assembly showing glass vessel attached to pressure gauge and valve system. A polytetrafluoroethylene barrier inside of the glass cylinder prevents corrosive sulfide environment from reacting with the borosilicate glass* ***B.*** *Static reactor placed inside heating block.*

Single Pass Flow Through (SPFT)

- Designed to simulate realistic conditions if brine ever penetrated the WIPP repository
- Fresh SGWB continuously pumped into reactors
- Conducted in glovebox under nitrogen atmosphere at 90°C

Single Pass Flow Through

- Steel coupons polished to mirror like 1μm grit finish
- RTV silicone applied to several areas to preserve pristine surface during experiment
- Coupons placed into Teflon reactors sitting inside of a heat block
- Hydrogen traps placed within the system for generated gas collection

Single Pass Flow Through

Figure 2. *Glovebox setup for Single Pass Flow Thru Experiments. The hanging IV bags contain the experimental solutions. Reaction vessels are covered in insulating foam and cannot be seen.*

Single Pass Flow Through

Schematic of flow through set up. The IV bag is full of solution which is then pumped into the reaction reservoir containing the steel coupon. Waste is collected to ensure a continuous source of fresh solution.

Single Pass Flow Through

Table 2. *List of solutions for each reactor in the Single Pass Flow Through setup*

Reactor Number	Solution	Sulfide
1	SGWB	-
2	SGWB	-
3	SGWB	-
4	SGWB	0.001m NaHS
5	SGWB	0.005m NaHS
6	SGWB	0.010m NaHS
7	Deionized Water	-
8	Deionized Water	-
9	Deionized Water	-
10	Deionized Water	0.0001m NaHS

Corrosion Rate Determination by Fe Release

- ICP-MS used to analyze solution for Iron content

$$-r_t = \frac{(C_{i,in} - C_{i,out}) \times Q_{s,t}}{v_i \times A_{s,t}}$$

$r_t = mass\ flux\ of\ an\ element\ at\ time\ t\ (\frac{g}{m^2 * d})$

$C_{i,in} = the\ concentration\ of\ the\ element\ i\ into\ the\ reactor\ (\frac{g}{m^3})$

$C_{i,in} = the\ concentration\ of\ the\ element\ i\ out\ of\ the\ reactor\ (\frac{g}{m^3})$

$Q_{s,t} = mass\ flow\ rate\ of\ effluent\ over\ the\ coupon\ at\ time\ t\ (\frac{L}{d})$

$v_i = the\ mass\ fraction\ of\ the\ elment\ i\ in\ the\ steel\ coupon\ (\frac{g\ element}{g\ steel})$

$A_{s,t} = the\ area\ of\ the\ coupon\ at\ time\ t\ (m^2)$

Corrosion Rate Determination by $H_2(g)$ Release

- Hydrogen gas generated during the experiments was trapped in graduated cylinders
- Bottles under vacuum were used to collect samples for GC-MS analysis
- Results were inconclusive

Corrosion Rate Determination by Weight Loss

- After experiment termination, steel coupons cleaned according to ASTM G1-03.

- Weights after each cleaning cycle were recorded to calculate weight loss

Corrosion Rate Determination by Weight Loss

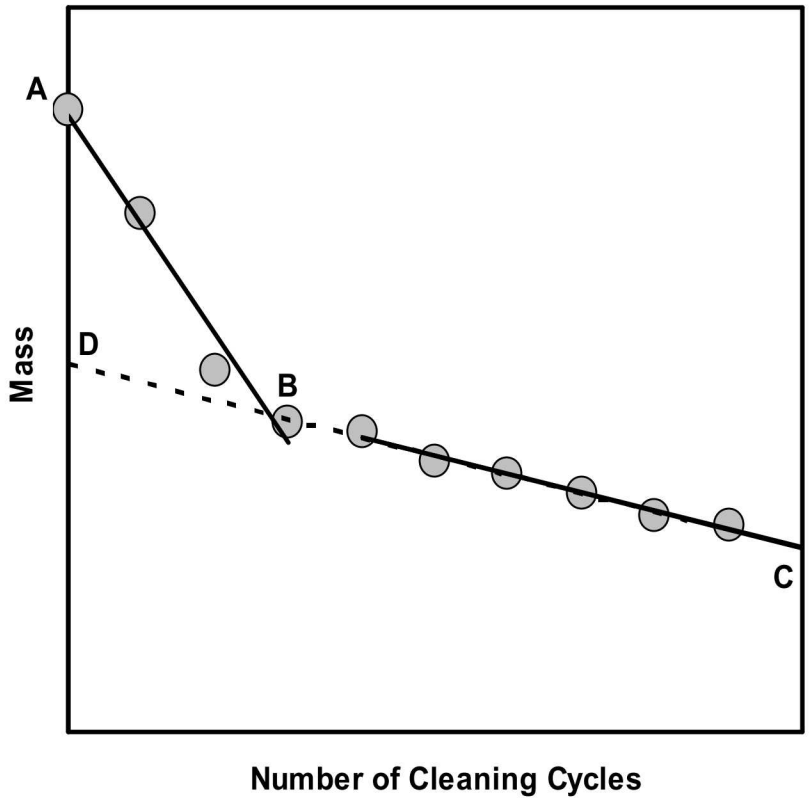

Figure 3. *Plot of weight loss measurement after each cleaning cycle. Line segment AB represents the loss of corrosion products. BC represents loss of pristine steel. BC is extrapolated backwards to point D which is the final projected mass loss of the steel.*

Corrosion Rate Determination by Weight Loss

- Using Equation 2, surface retreat in μm/yr can be calculated

$$rate\ (r) = \frac{W \times 87.6}{SA \times t \times \rho} \times 1000$$

$$W = mass\ loss\ (mg)$$
$$SA = surface\ area\ (cm^2)$$
$$t = time\ exposed\ to\ corrosion\ conditions\ (hrs)$$
$$\rho = steel\ density\ \left(\frac{g}{cm^3}\right)$$

Corrosion Rate Determination by Interferometry

- Interferometry is a novel technique for corrosion studies to directly measure surface retreat
- Uses refracted light beams to measure minute differences in height
- Once RTV masks removed, step change in height can be measured

Corrosion Rate Determination by Interferometry

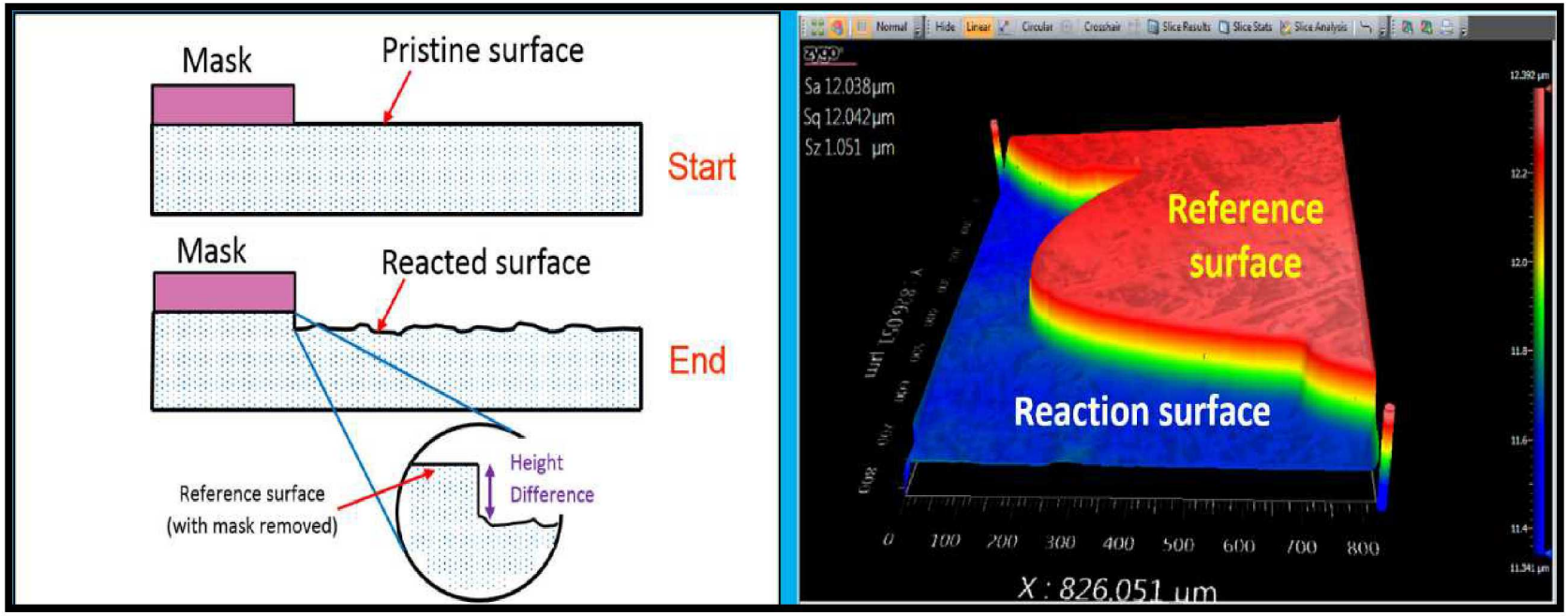

Figure 4. *An illustration of interferometry technique. A mask (RTV sealant) is applied to the surface of a steel coupon and placed into a reactor. Solution reacts with the exposed surface of steel, causing dissolution and surface retreat. The mask is then removed revealing the pristine surface. This change in height can then be measured with interferometry.*

Electrochemical Set-up

- Electrochemical tests were run to determine rates relatively quickly
- Set-up was created to mimic SPFT conditions at 90°C and a nitrogen environment.
- A Gamry Multiport Corrosion Cell Kit was used
- Heating jacket connected to Omega temperature controller was used to maintain temperature.

Electrochemical Set-up

Figure 5. *Electrochemical cell set up with heating jacket.*

Results

Single Pass Flow Through

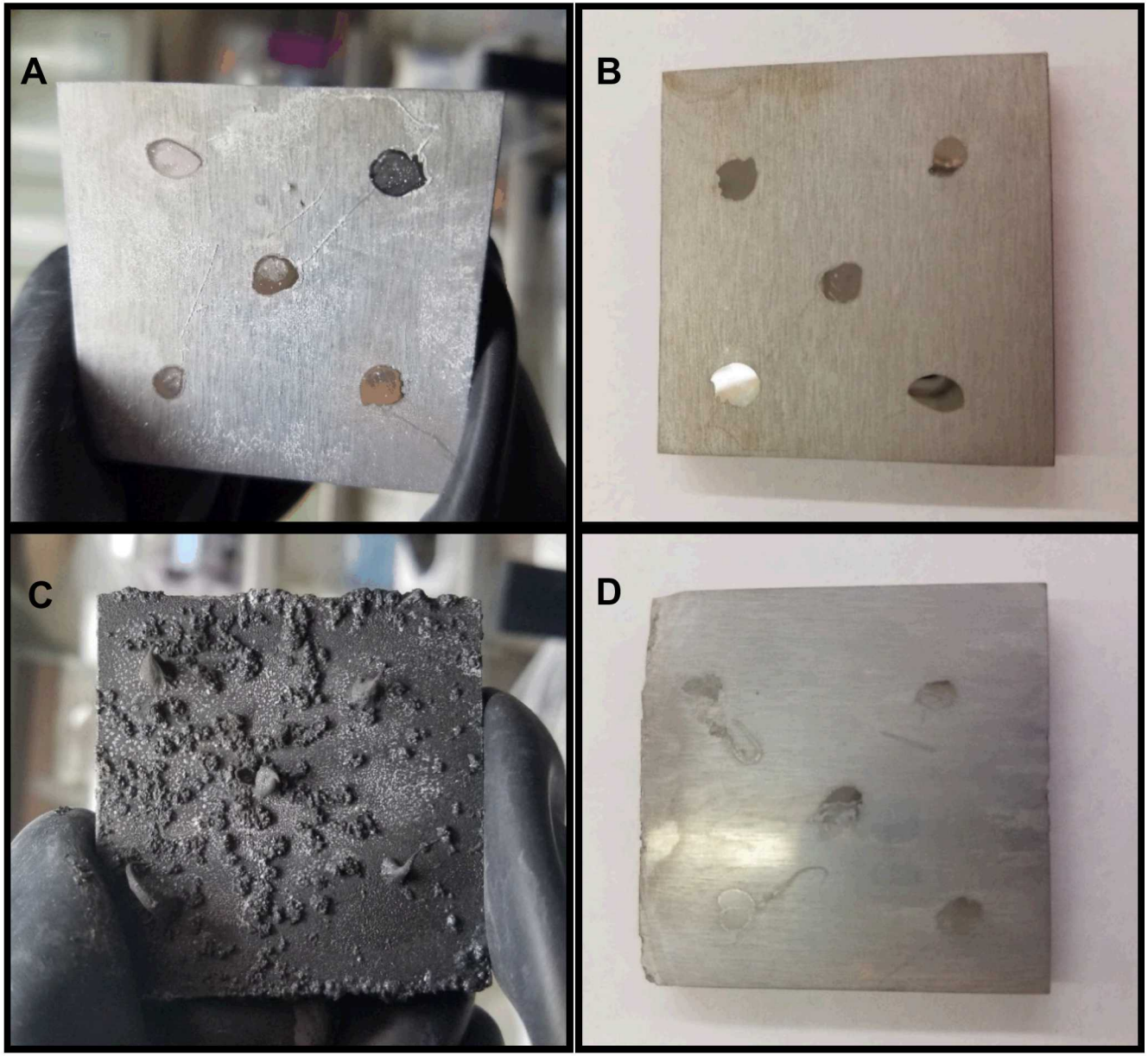

Figure 6. A. Corroded coupon from reactor 2 (SGWB) before cleaning. B. Coupon from reactor 2 after cleaning. C. Coupon from Reactor 5 (SGWB + 5 mmol NaHS) before cleaning. D. Coupon from Reactor 5 after cleaning. Note the roughening of the left edge of the coupon, this edge was at the bottom of the reactor where corrosion products collected and exhibited greater pitting. Coupons are 50 mm across.

Weight Loss

Table 3. *List of Single Pass Flow Thru corrosion rates as determined by weight loss.*

Reactor	Solution	Corrosion Rate (um/yr)
1	SGWB	No Coupon Present
2	SGWB	13.63
3	SGWB	11.29
4	SGWB + 1 mmol NaHS	16.05
5	SGWB + 5 mmol NaHS	Coupon Sacrificed for Characterization
6	SGWB + 10 mmol NaHS	73.49
7	DI Water	0.47
8	DI Water	0.65
9	DI Water	0.78
10	DI Water + 1 mmol NaHS	Not Measured Yet
11	DI Water + 5 mmol NaHS	Not Measured Yet

Interferometry

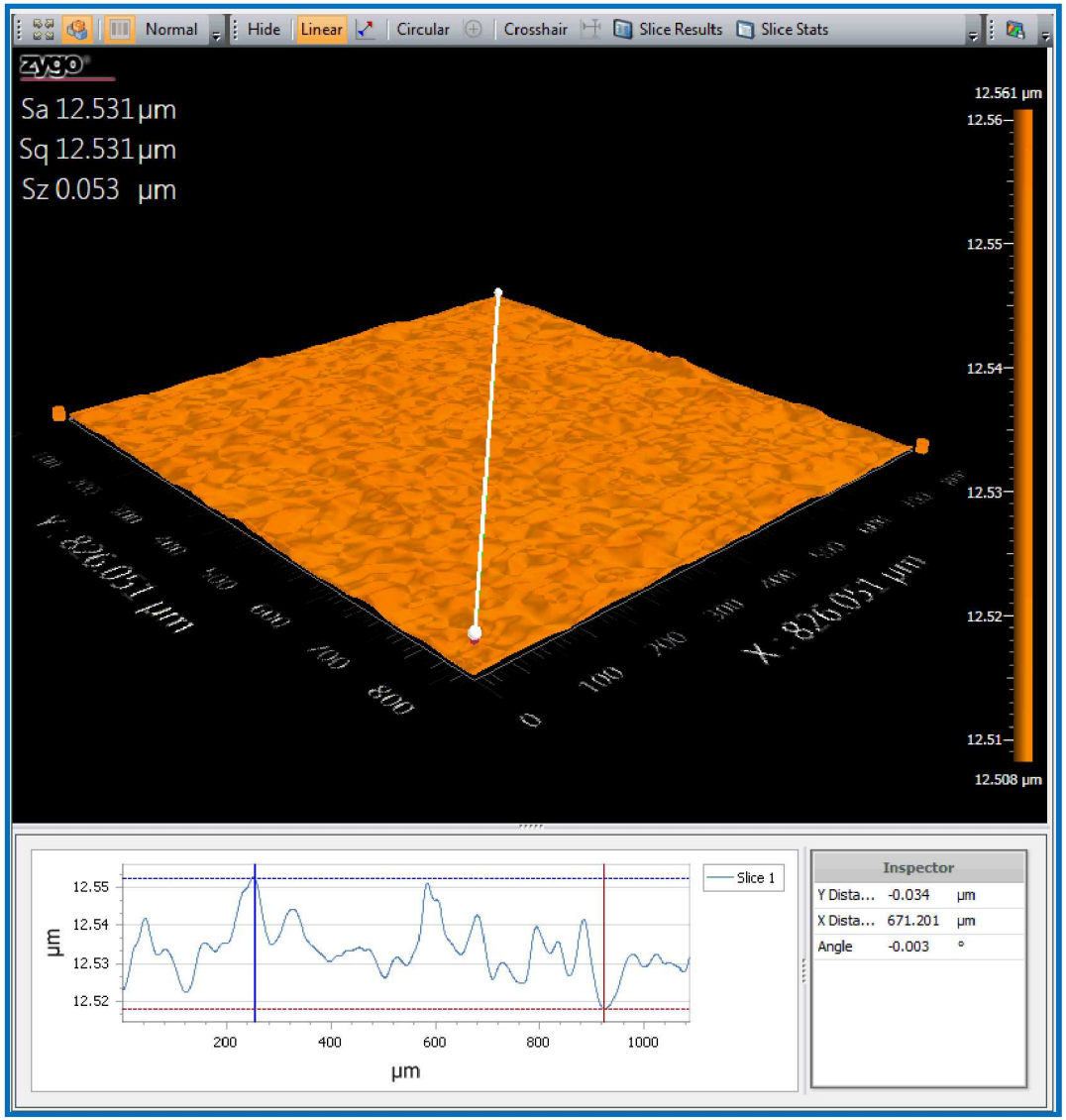

Figure 7. *Interferometry image of pristine surface before initiation of corrosion test.*

Interferometry

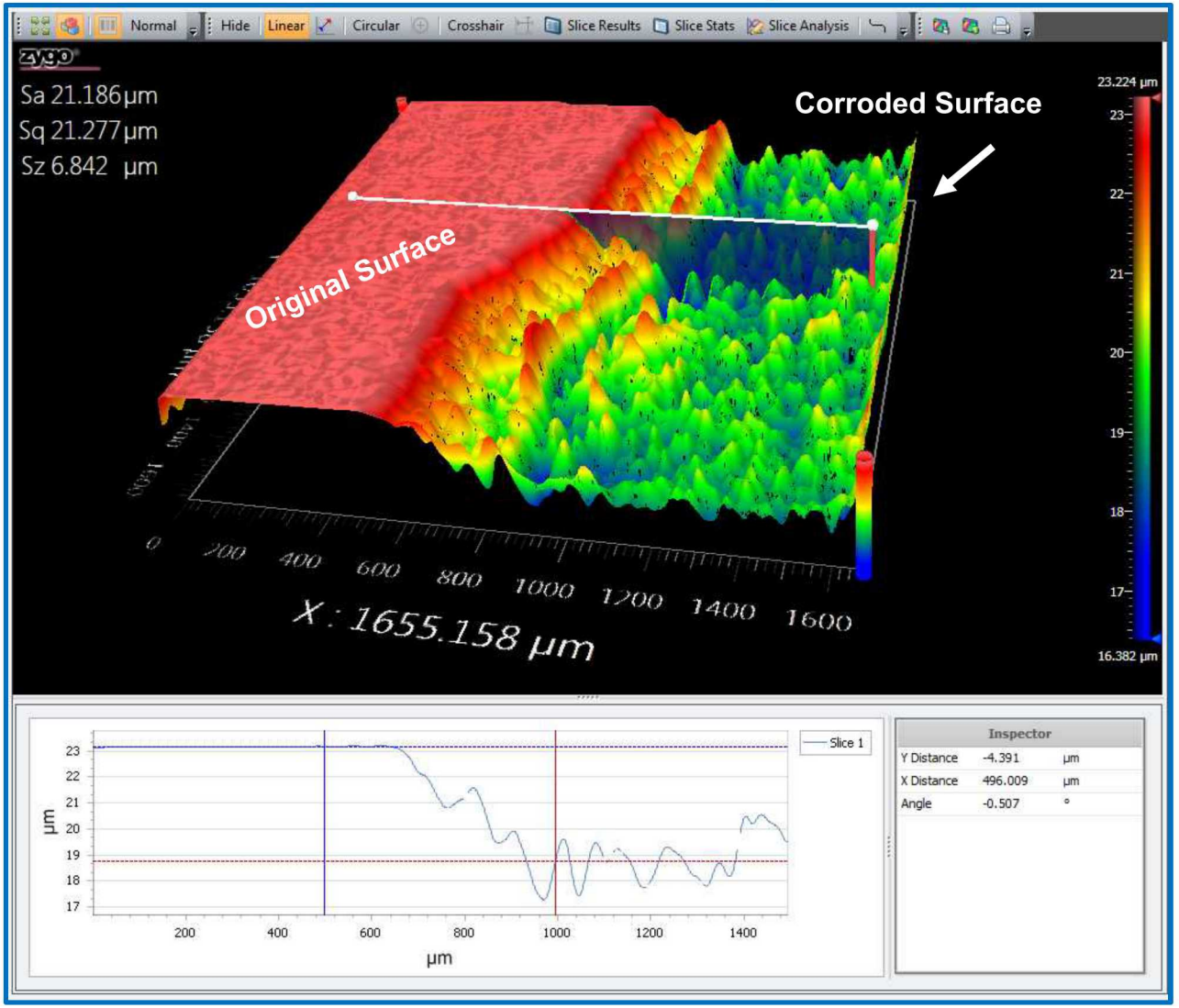

Figure 8. *Interferometry image of coupon from Reactor 4. The masked surface can be seen as the red region and the corroded surface as the roughened green region.*

Interferometry

Table 4. *List of Single Pass Flow Thru Rates as determined by interferometry.*

Reactor	Solution	Corrosion Rate (um/yr)
1	SGWB	No Coupon Present
2	SGWB	11.95
3	SGWB	11.07
4	SGWB + 1 mmol NaHS	5.49
5	SGWB + 5 mmol NaHS	Coupon Sacrificed for Characterization
6	SGWB + 10 mmol NaHS	1.38

Electrochemical Impedance Spectroscopy

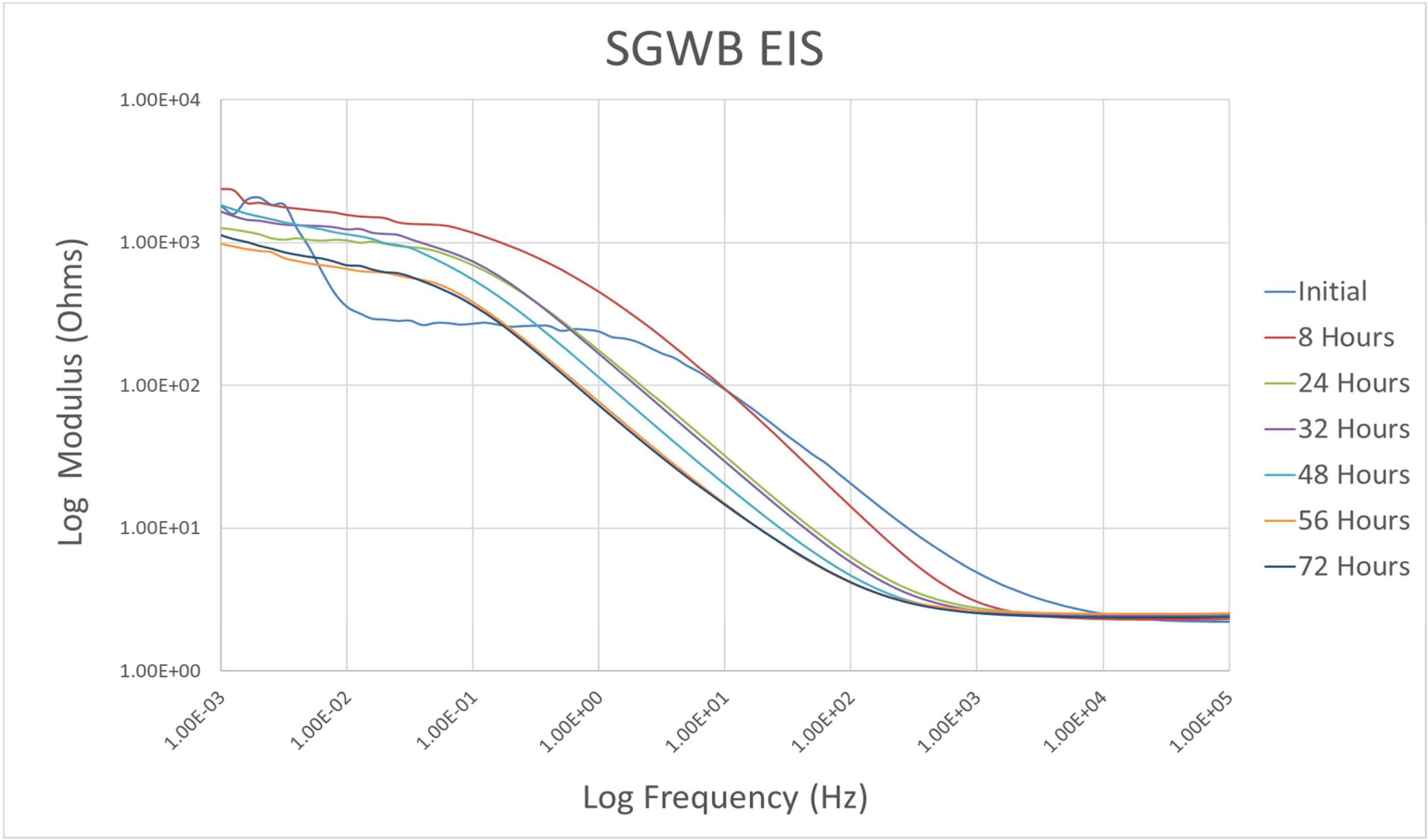

***Figure 9**. Bode plot from the Electrochemical Impedance test in SGWB solution.*

Potentiodynamic Polarization

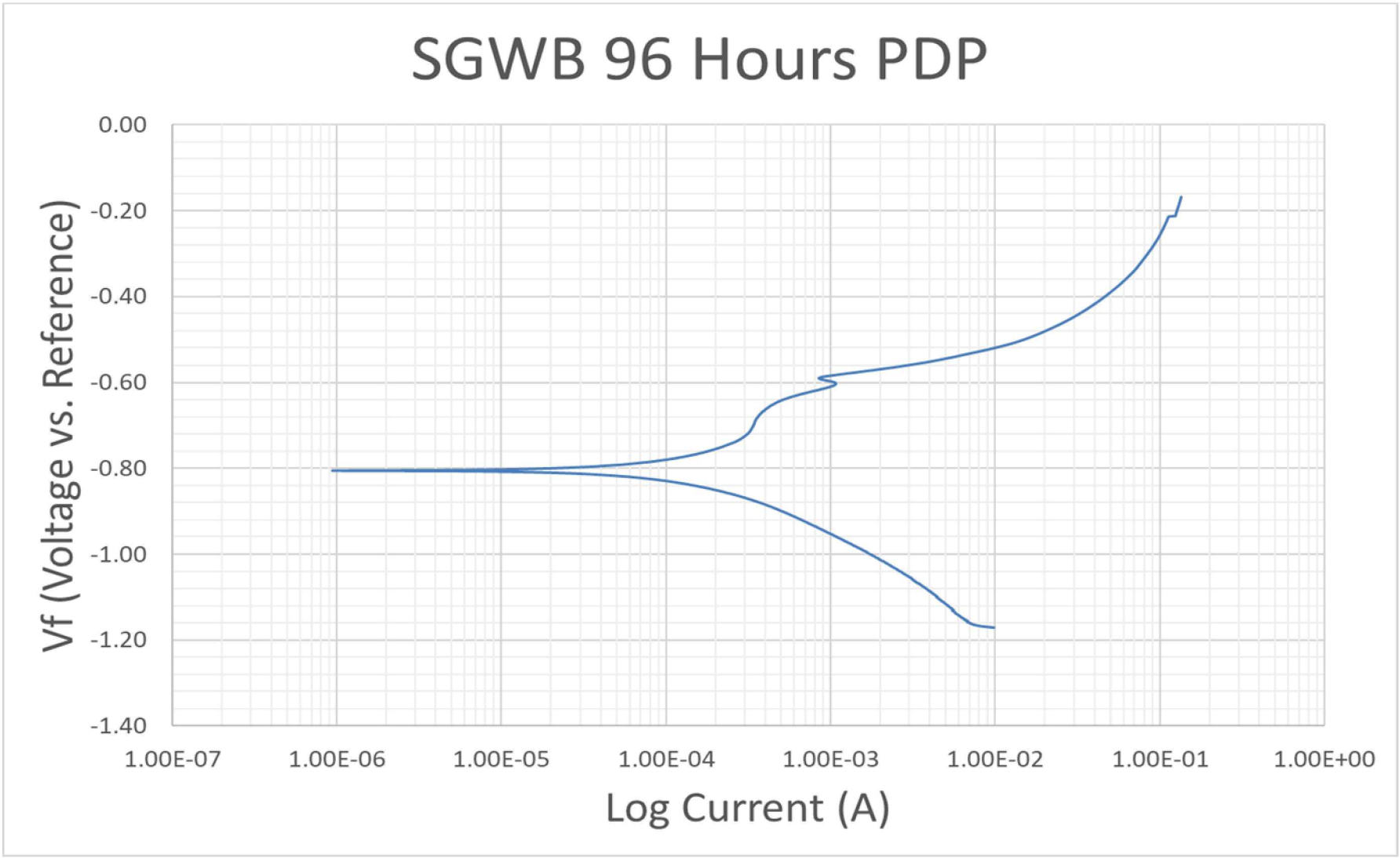

Figure 10. *Tafel plot from Potentiodynamic Polarization test in SGWB solution. Test was conducted after completion of the EIS tests at 96 hours.*

Electrochemical Corrosion Rates

$$Icorr = \frac{B}{Rp}$$

$$Icorr = \ Corrosion\ Current\ \left(\frac{\mu A}{cm^2}\right)$$
$$B = Stern - Geary\ coefficient\ (V/decade)$$
$$Rp = Resistance\ Polarization\ (ohm * cm^2)$$

The Stern Geary coefficient is extracted from the Tafel plot and is calculated using the equation below.

$$B = \frac{Ba * Bc}{2.303(Ba + Bc)}$$

$$Ba = Annodic\ Slope\ \ (V/decade)$$
$$Bc = Cathodic\ Slope\ (V/decade)$$

Electrochemical Corrosion Rates

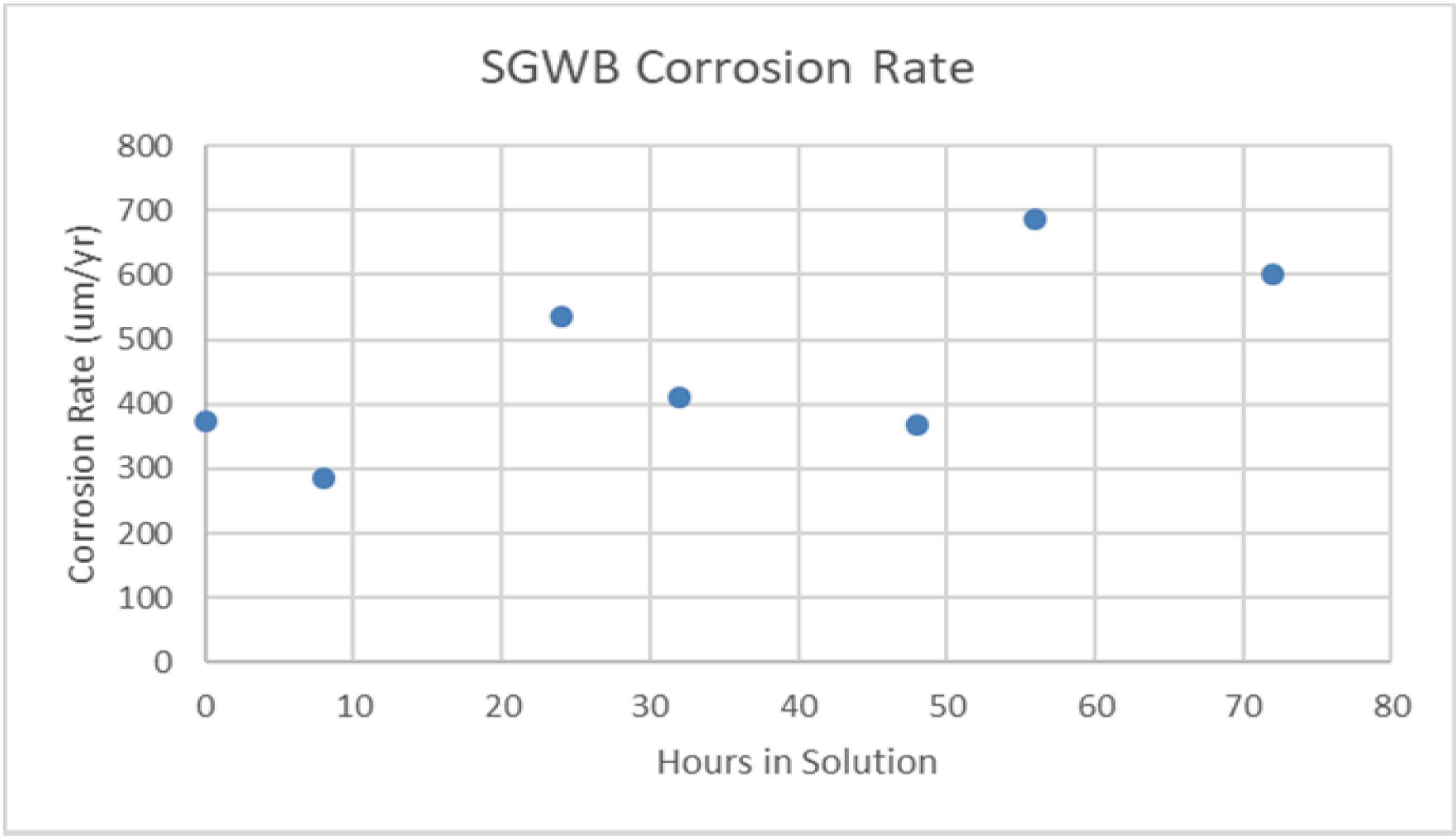

***Figure 11**. Corrosion rates extracted from the EIS tests plotted over time.*

Characterization

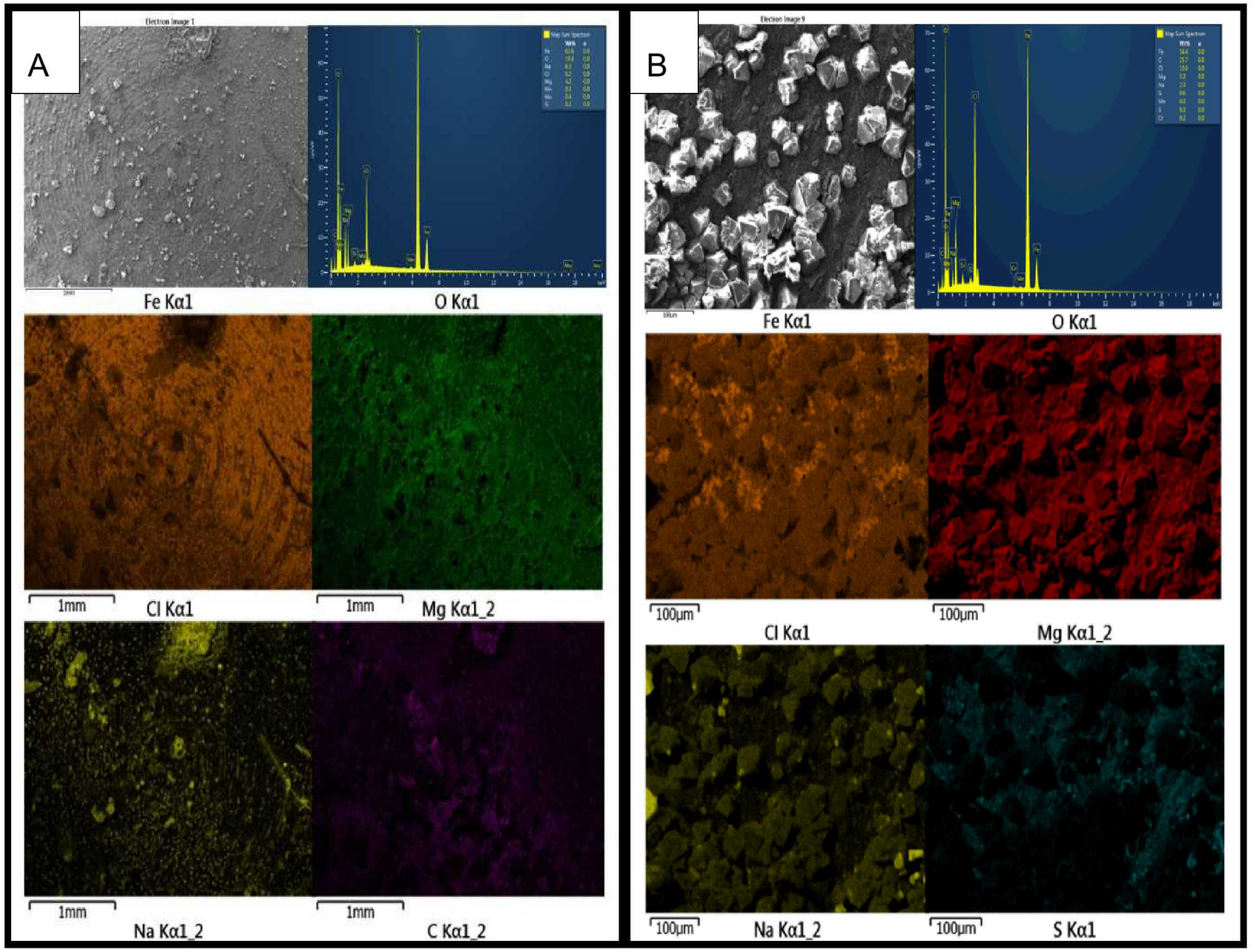

***Figure 12**. A. EDS scan of coupon from Reactor 2 (SGWB). B. EDS Scan of coupon from Reactor 4 (SGWB + 1 mmol NaHS).*

Characterization

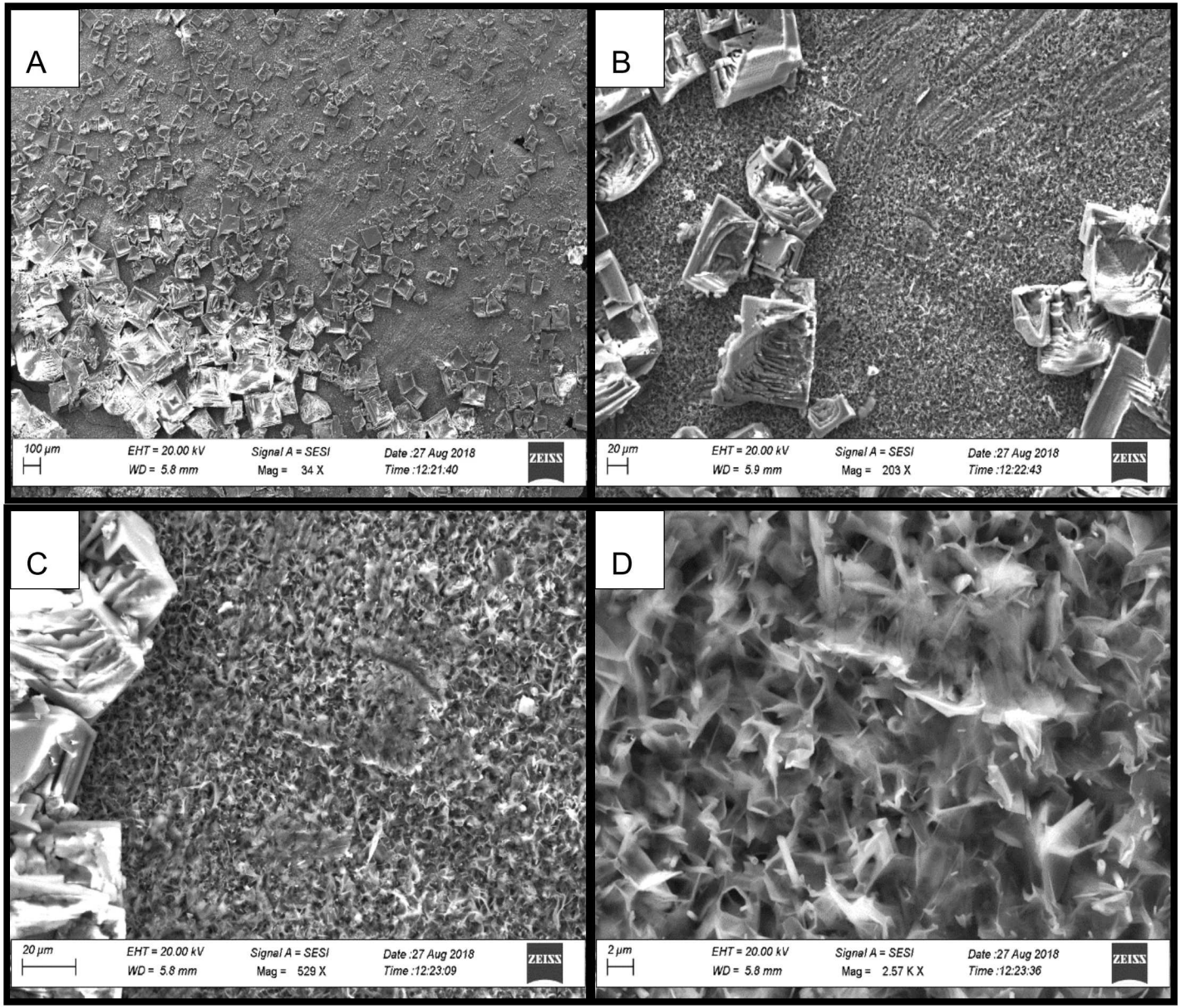

Figure 13. *SEM image of Coupon from Reactor 2 (SGWB). A. 34X Magnification, salt crystals present. B. 203X magnification, hopper formation can be seen in the NaCl crystals, finer corrosion layer becomes apparent. C. 529X Texture of corrosion product layer now visible. D. 2570X Zoomed in look at corrosion product layer.*

Characterization

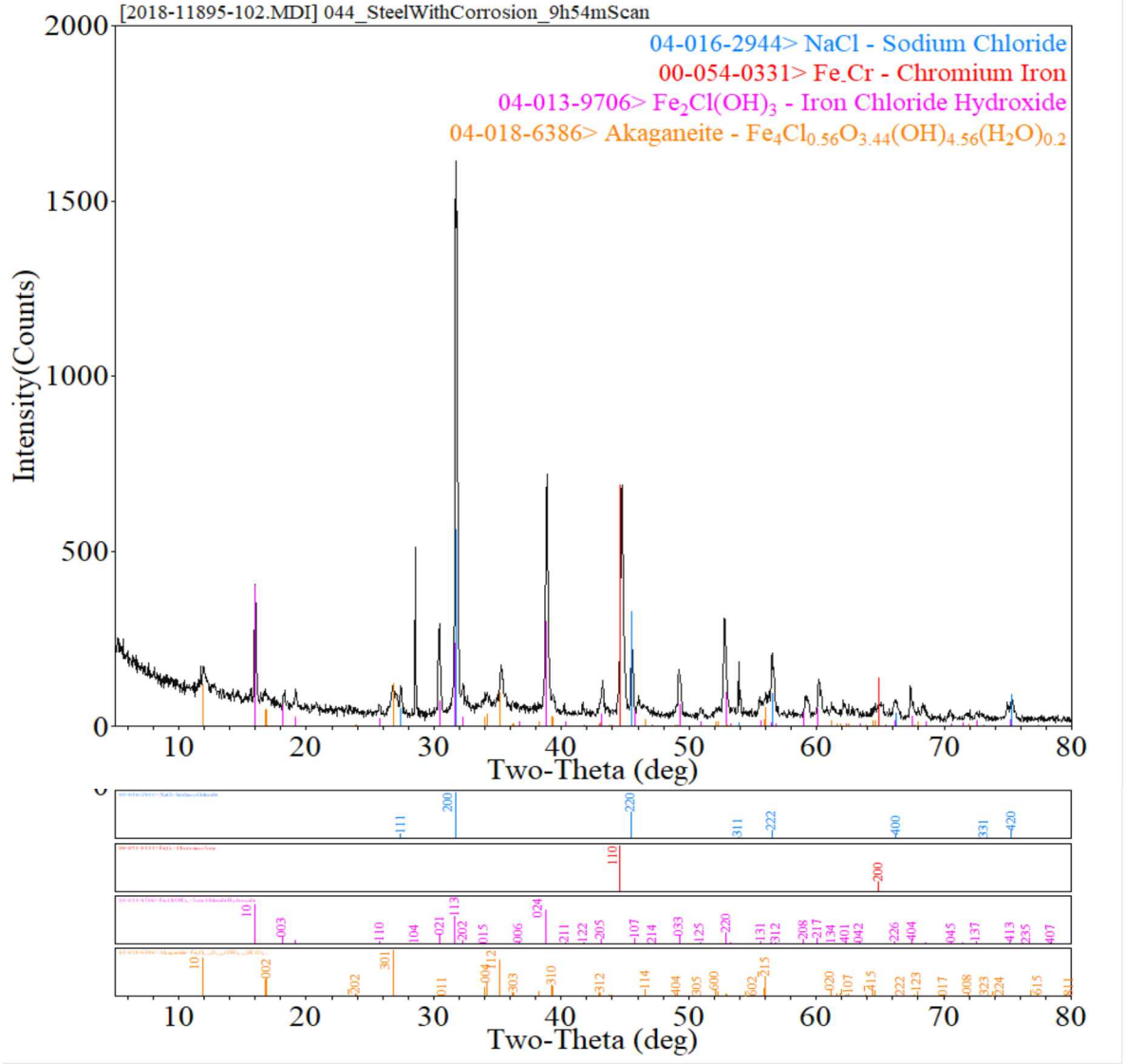

***Figure 14**. XRD diffractogram of corrosion products from Reactor 2 (SGWB) coupon.*

Characterization

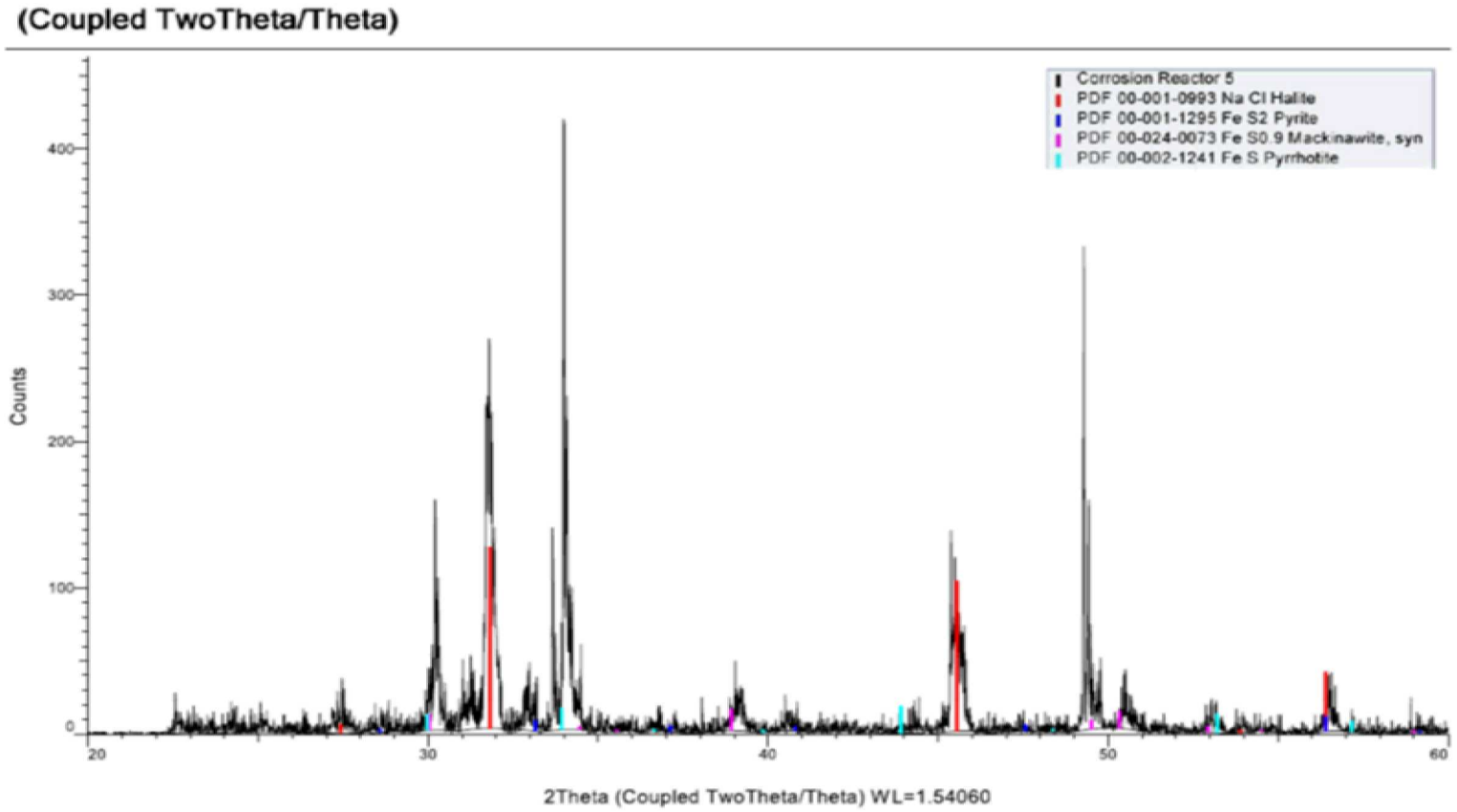

Figure 15. *XRD diffractogram of corrosion products from Reactor 5 (SGWB + 5 mmol NaHS). Various compounds such as Pyrite, Mackinawite, and Pyrrhotite present.*

Characterization

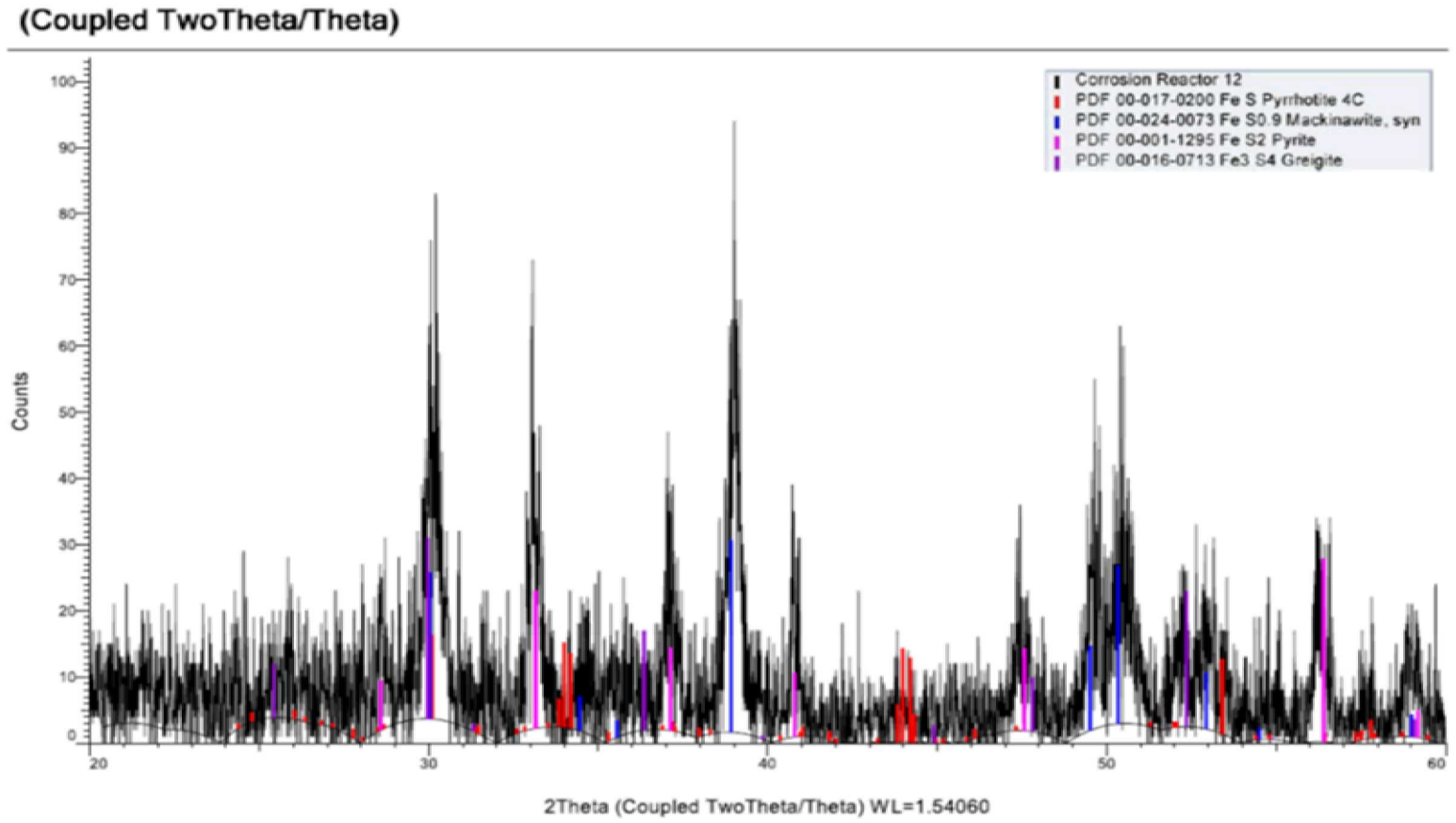

Figure 16. *XRD diffractogram of corrosion products from Reactor 12 (DI water + 10 mmol NaHS). Pyrrhotite, Mackinawite, Pyrite, and Greigite present.*

Characterization

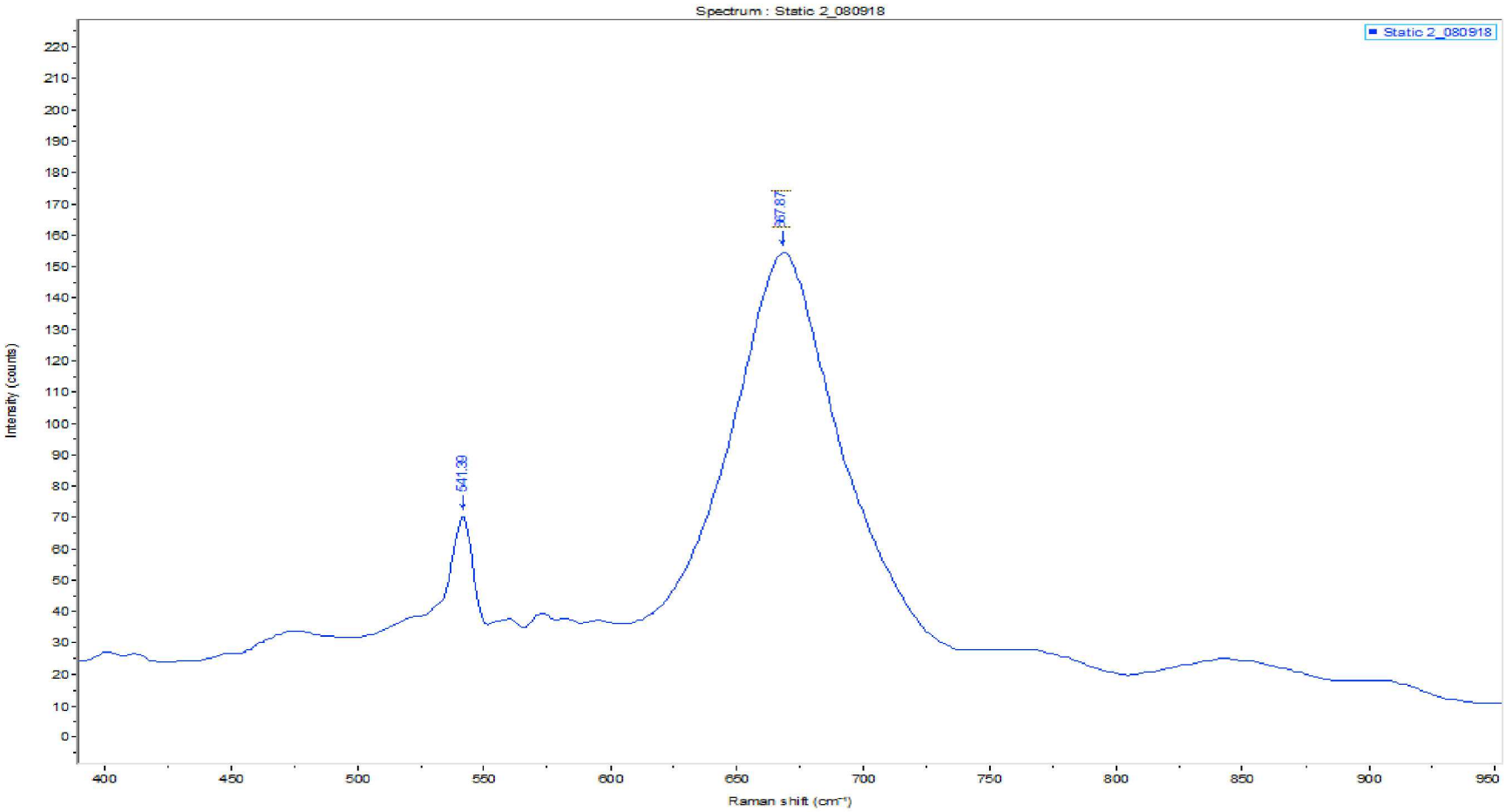

Figure 17*. Raman spectroscopy analysis of corrosion products form Reactor 2 (SGWB). Peaks at 540 cm^{-1} and 670 cm^{-1} are characteristic of Magnetite.*

Characterization

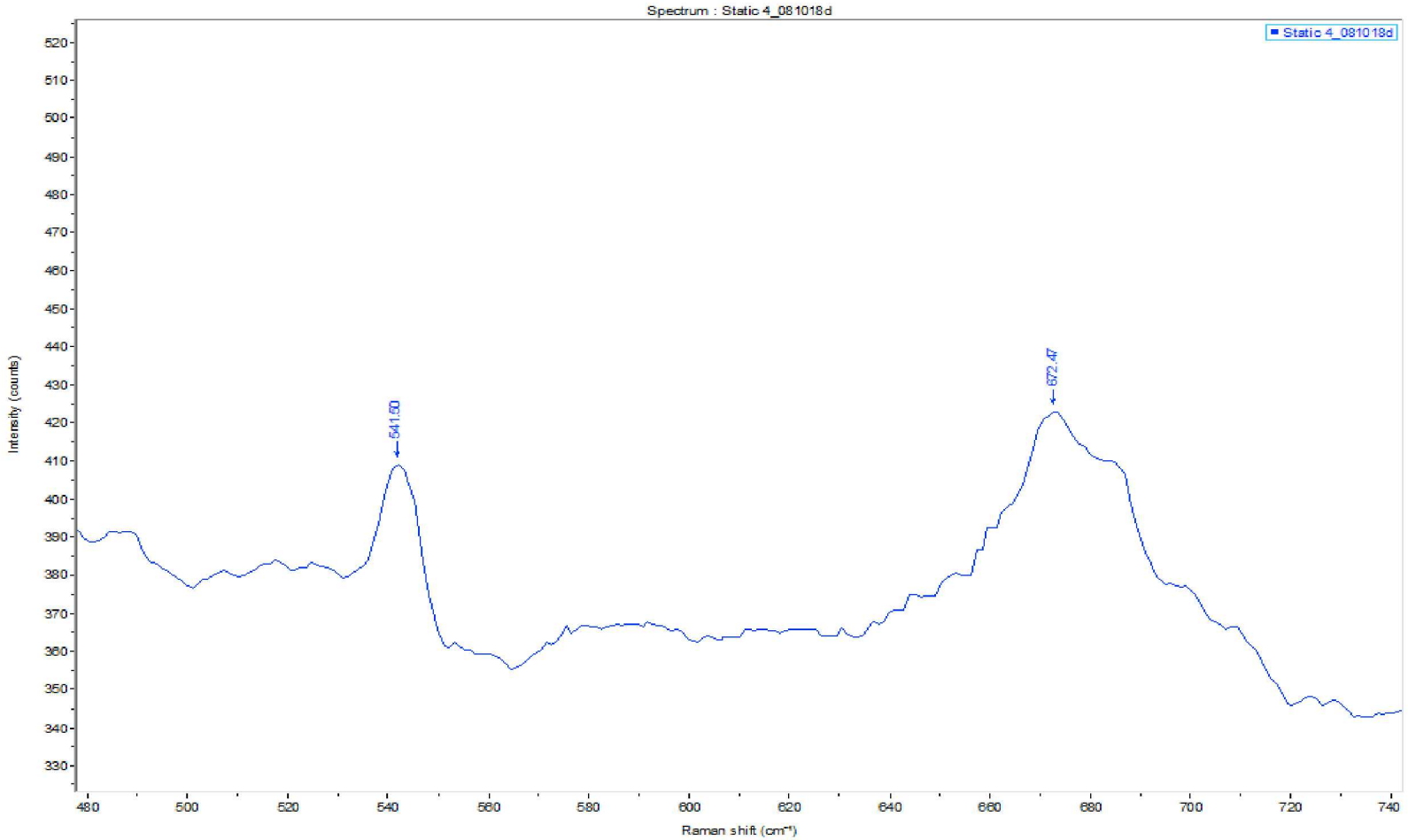

***Figure 18**. Raman spectroscopy analysis of corrosion production from Reactor 4 (SGWB + 1 mmol NaHS). Peaks at 540 cm^{-1} and 670 cm^{-1} are characteristic of Magnetite.*

Characterization

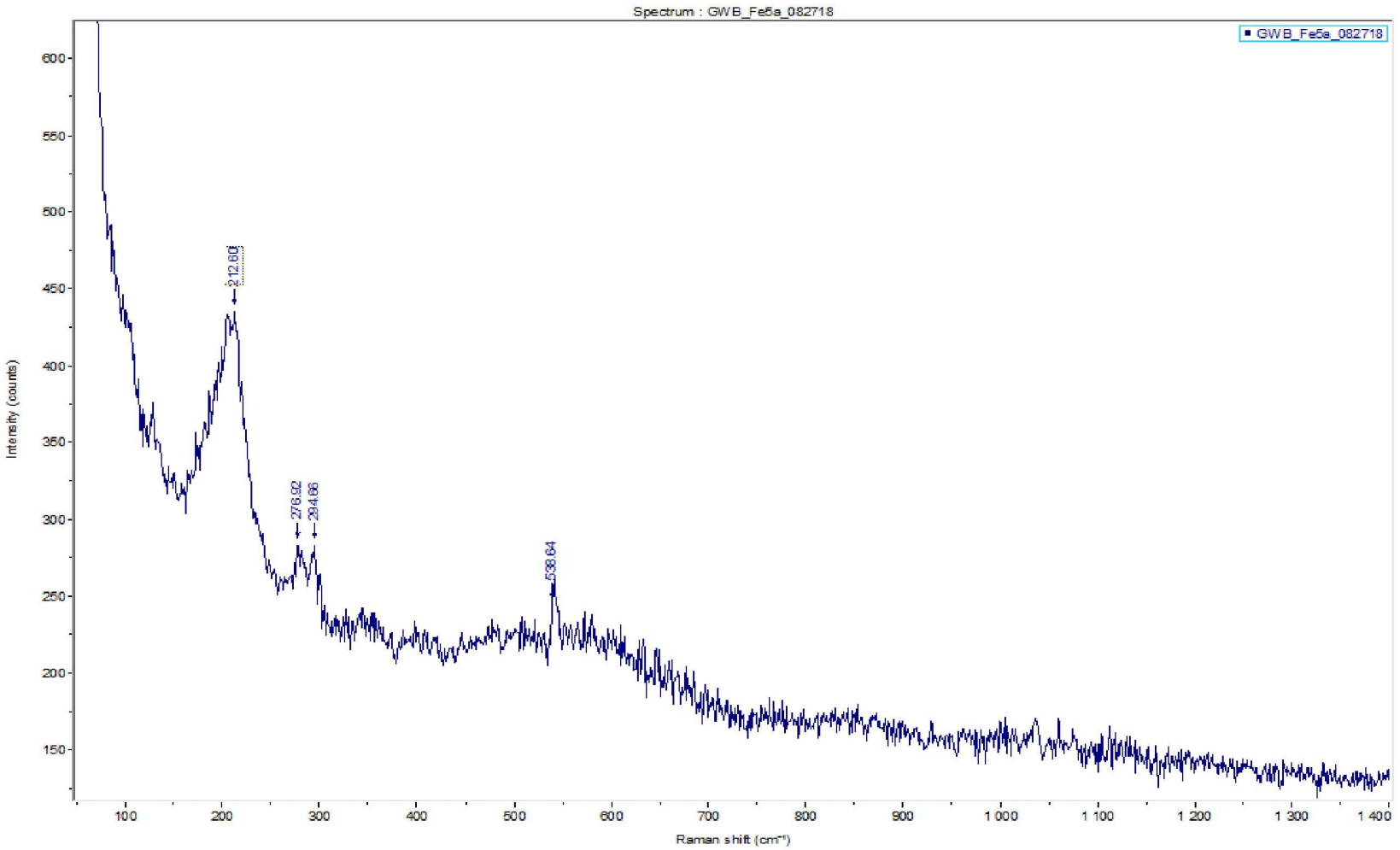

Figure 19. *Raman spectroscopy analysis of corrosion production from Reactor 5 (SGWB + 5 mmol NaHS). Peaks at 212 cm-1 and 276 cm-1 are characteristic of Mackinawite.*

Characterization

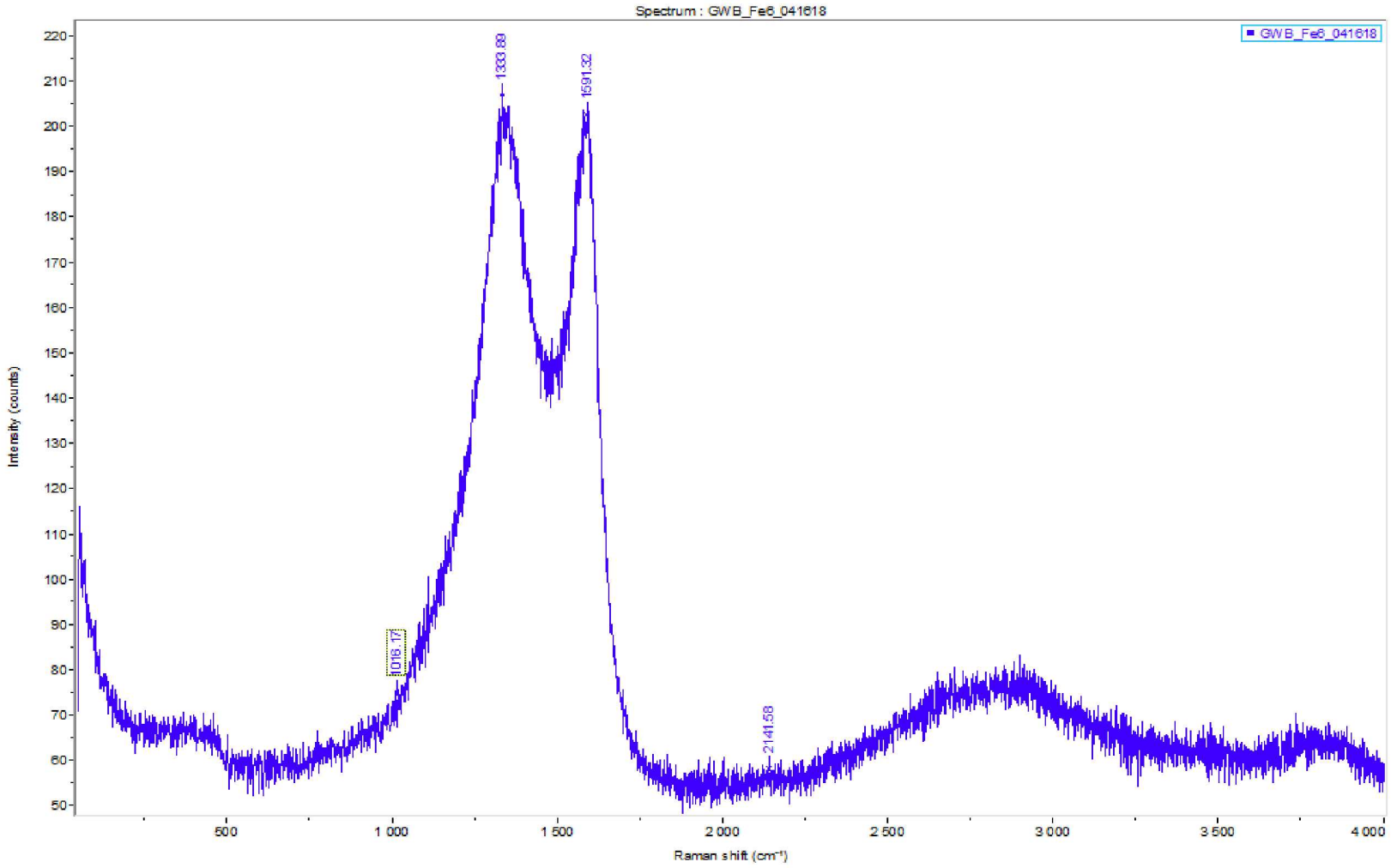

Figure 20. *Raman spectroscopy analysis of corrosion production from Reactor 6 (SGWB + 10 mmol NaHS). Peaks at 1333 cm^{-1} and 1591 cm^{-1} are characteristic of Graphite.*

Proposed Research

- The most recent set of SPFT experiments includes work for KIT. These tests will be further analyzed for Fe release to help understand the corrosion mechanism over time

***Table 5**. List of solutions and steel types for KIT SPFT experiments.*

Sample ID	Brine Solution	Coupon Composition	Solution 3 Composition
KIT-F1	5 M NaCl	Graphite steel	▪ 5 M NaCl ▪ 0.0188 M CaCl2 •2H2O ▪ 0.0188 M Na2SO4 ▪ 0.015 M K2SO4 ▪ 0.015 M MgSO4 •7H2O
KIT-F2	3.4 $MgCl_2$	Graphite steel	
KIT-F3	Solution 3	Graphite steel	
KIT-F4	5 M NaCl	Cr-Ni steel	
KIT-F5	3.4 $MgCl_2$	Cr-Ni steel	
KIT-F6	Solution 3	Cr-Ni steel	

Proposed Research

- Complete analysis on all SPFT experiments
- Complimentary electrochemical tests for all SPFT experiments (excluding KIT conditions)
- Vary temperature on electrochemical tests to create a better model

Summary

- SPFT experiments are a useful method for realistic simulation
- Numerous techniques will provide a broad understanding of corrosion mechanisms under these conditions
- A sufficient model will be obtainable after completion of experimentation and analysis

References

Cui, D. and Eriksen T. E. (1996) Reduction of pertechnetate in solution by heterogeneous electron transfer from Fe(II)-containing geological material. Environmental Science and Technology 30, 2263-2269.

Daoud, D., Douadi, T., Hamani, H., Chafaa, S and Al-Noaimi, M. (2015) Corrosion inhibition of mild steel by two new S-heterocyclic compounds in 1 M HCl: Experimental and computational study. Corrosion Science 94, 21-37.

Desimone, M. P., Gordillo, G. and Simison, S. N. (2011) The effect of temperature and concentration on the corrosion inhibition mechanism of an amphiphilic amido-amine in CO_2 saturated solution. Corrosion Science 53, 4033-4043.

Felmy, A. R., Moore, D. A., Qafoku, O., Buck, E., Conradson, S. D., Ilton, E. S. (2013) Heterogeneous reduction of (PuO_2)-Pu-239 by aqueous Fe(II) in the presence of hematite. Radiochimica Acta 10, 701-710.

Génin, J. M. R., Refait, P., Bourrié, G., Abdelmoula, M. and Trolard, F. (2001) Structure and stability of the Fe(II)-Fe(III) green rust "fougerite" mineral and its potential for reducing pollutants in soil solutions. Applied Geochemistry 16, 559-570.

Gui, J and Devine, T.M., Obtaining surface-enhanced raman spectra from the passive film on iron, Journal of Electrochemical Society 138, 1376.

Herbert, R.B., Pratt, A.R., Blowes, D.W., Benner, S.G., (1998) Surface oxidation of iron monosulphide: an X-ray photoelectron spectroscopic study. Mineralogical Magazine 64A, 608-609.

Kaneko, M., Miura, N., Fujiwara, A. and Yamamoto, M. (2004) Evaluation of Gas Generation Rate by Metal Corrosion in the Reducing Environment. Radioactive Waste Management Funding and Research Center (RWMC) Engineering Report RWMC-TRE-03003, Tokyo, Japan.

References

Liu, M., Wang, J., Ke, W. and Han, E.-H. (2014) Corrosion behavior of X52 anti-H2S pipeline steel exposed to high H2S concentration solutions at 90 °C. Journal of Materials Science and Technology 30, 504-510.

Mobin, M. and Masroor, S. (2012) Alkanediyl-□,□-bis (dimethyl cetylammonium bromide) gemini surfactants as novel corrosion inhibitors for mild steel in formic acid. Materials Research 15, 837-847.

Refait, P. and Genin, J.M.,(1997) The mechanisms of oxidation of ferrous hydroxychloride β-Fe2(OH)3Cl in aqueous solution: the formation of akageneite vs. goethite, Corrosion Science 39, 539-553.

Refait, P., Abdelmoula, M. and Génin, J. M. (1998) Mechanisms of formation and structure of green rust one in aqueous corrosion of iron in the presence of chloride ions. Corrosion Science 40, 1547-1560.

Remazeilles, C. and Refait, P. (2008) Formation , fast oxidation and thermodynamic data of Fe(II) hydroxychlorides, Corrosion Science 50 (3), 856-864.

Roselle, G. T. (2011) Analysis Plan for Determination of Gas Generation rates from Iron/Lead Corrosion Experiments (AP-151, Rev. 0). Sandia National Laboratories Waste Isolation Pilot Plant.

Roselle, G. T. (2009) Iron and Lead Corrosion in WIPP-Relevant Conditions: Six Month Results. Milestone Report, October 7, 2009. ERMS 546084. Sandia National Laboratories, Carlsbad, NM.

Roselle, G. T. (2010) Iron and Lead Corrosion in WIPP-Relevant Conditions: 12 Month Results. Milestone Report, October 14, 2010. ERMS 55483. Sandia National Laboratories, Carlsbad, NM.

Schlegel, M. L., Bataillon, C., Bruker, F., Blanc, C., Prêt, D., Foy E. and Chorro, M. (2014) Corrosion of metal iron in contact with anoxic clay at 90 °C: Characterization of the corrosion products after two years of interaction. Applied Geochemistry 51, 1–14.

References

Sherar, B. W. A., Keech, P. G., Qin, Z., King, F. and Shoesmith, D. W. (2010) Nominally anaerobic corrosion of carbon steel in near-neutral pH saline environments. Corrosion 66, 045001-1.

Sherar, B. W. A., Power, I. M., Keech, P. G., Mitlin, S., Southam, G. and Shoesmith, D. W. (2011) Characterizing the effect of carbon steel exposure in sulfide containing solutions to microbially induced corrosion. Corrosion Science 53, 955-960.

Sherar, B. W. A., Keech, P. G., Noel, J. J., Worthingham, R. G. and Shoesmith, D. W. (2013) Effect of sulfide on carbon steel corrosion in anaerobic near-neutral pH saline solutions. Corrosion 69, 67-76.

Smart, N. R., Rance, A. P., Fennell, P. A. H. and Kursten B. (2014) Effect of sulphur species on anaerobic corrosion of carbon steel in alkaline media. Corrosion Engineering, Science and Technology 49, 473-479.

Soliman, S. A., Metwally, M. S., Selim, S. R., Bedair, M. A. and Abbas, M. A. (2014) Corrosion inhibition and adsorptive behavior of new Schiff base surfactant on steel in acidic environment: Experimental and theoretical studies. Journal of Industrial and Engineering Chemistry 20, 4311-4320.

Telander, M. M. and Westerman, R. E. (1993) Hydrogen Generation by Metal Corrosion in Simulated Waste Isolation Pilot Plant Environments". SAND92-7347. ERMS 223456. Sandia National Laboratories, Albuquerque, NM.

Telander, M. M. and Westerman, R. E. (1997) Hydrogen Generation by Metal Corrosion in Simulated Waste Isolation Pilot Plant Environments". SAND96-2538. Sandia National Laboratories, Albuquerque, NM.

References

Van Soest, G. (2012) Performance Assessment Inventory Report – 2012. LA-UR-12-26643. Carlsbad, NM: Los Alamos National Laboratory.

Viollier, E., Inglett, P. W., Hunter, K., Roychoudhury, A. N. and Van Cappellen, P. (2000) The ferrozine method revisited: Fe(II)/Fe(III) determination in natural waters. Applied Geochemistry 15, 785-790.

Wu, L., Beauregard, Y., Qin, Z., Rohani, S. and Shoesmith, D. W. (2012) A model for the influence of steel corrosion products on nuclear fuel corrosion under permanent disposal conditions. Corrosion Science 61, 83-91.

Yazdanfar, K., Zhang, X., Keech, P. G., Shoesmith, D. W. and Wren, J. C. (2010) Film conversion and breakdown processes on carbon steel in the presence of halides. Corrosion Science 52, 1297-1304.

Zachara, J. M., Heald, S. M., Jeon, B.-H., Kukkudapu, R. K., Liu, C., McKinley, J. P., Dohnalkova, A. C. and Moore, D. A. (2007) Reduction of pertechnetate [Tc(VII)] by aqueous Fe(II) and the nature of solid phase redox products. Geochimica et Cosmochimica Acta 71, 2137-2157.

Zhi-Rong, W., Juncheng, J., Xuhai, P. (2002) Experimental and theoretical study on erosion of tanks containing coking gasoline. Journal of Petrochemical Universities 15, 65-69.